Received 5 April 2023; Accepted 6 June 2023
https://doi.org/10.22226/2410-3535-2023-4-281-285

Al-Ce alloy high cooling rate cells: a combined experimental and modeling strategy

R. B. Baraldi[1], D. da Silva[2], G. L. de Gouveia[2], A. Garcia[3], J. E. Spinelli[†,1]

[†]spinelli@ufscar.br

[1]Department of Materials Engineering, Federal University of São Carlos UFSCar, São Carlos, 13565-905, SP, Brazil
[2]Federal University of São Carlos, Graduate Program in Materials Science and Engineering, São Carlos, 13565-905, SP, Brazil
[3]Department of Manufacturing and Materials Engineering, University of Campinas, Campinas, 13083-860, SP, Brazil

Abstract: Al-Ce alloys are anticipated to offer high-temperature strength. In recent years, interest in these alloys has increased. While previous studies have looked into dendritic length-scale and how it relates to tensile properties, cellular growth has not been debated, despite its well-known significance. An in-depth study of Al-4, 6 and 10.1 wt.% Ce alloys involving microstructural analysis of Cu-mold centrifugal cast samples at various points, Vickers hardness, SEM and tensile properties was carried out here. α-Al cells were identified for a computed solidification velocity of 3.1 mm/s and a cooling rate of 155 K/s. These samples showed balanced tensile properties.

Keywords: Al-Ce alloys, cells, microstructure, solidification, centrifugal casting

1. Introduction

Ce strengthened Al alloys display extremely desirable features for a variety of applications, including high ductility, suitable mechanical properties at room temperature, exceptional high-temperature mechanical property retention, high casting defect tolerance, and good castability over a wide range of compositions [1–3]. These alloys may be economically viable for high volume industries like transportation because of the high availability and low cost of Ce, which makes its alloys a good alternative for vehicle light-weighting. The economics of rare earth mining also indicate a step toward stabilizing global production and diversifying the rare-earth supply chain by increasing demand for Ce, which is overproduced [3].

Because Ni has a diffusion coefficient in Al that is two orders of magnitude lower than that of Si or Mg, Al-Al3Ni eutectic has been employed to overcome the barrier of Al-Si and Al-Mg alloys developing thermally unstable precipitates and phases [1]. Despite this, the diffusion coefficient of Ce in Al is nearly four orders of magnitude lower than that of Ni in Al. This is a significant factor driving the development of novel heat-resistant Ce-containing Al alloys [2,3].

Previous research [4] showed that the microstructures of Al-Ce alloys are sensitive to solidification conditions. Solidification-dominated techniques, such as conventional casting [5] and laser additive manufacturing [6,7], have been typically used to fabricate Al-Ce alloys. As a matter of fact, more research must be carried out on intermediate-cooling rate solidification methods such as centrifugal casting, gravity casting, and die casting. In Al-12%Ce alloys processed by laser melting; eutectic structures were formed at melt-pool boundaries while α-Al dendritic/cellular structure prevailed near the melt-pool centerline [7]. It is worth noting that the solidification features of hypoeutectic Al-Ce alloys under various cooling conditions are not well mapped. Microstructures have been demonstrated as being a strategic link between cast alloys processing and their properties for binary Al-Fe, Al-Ni and Al-Si alloys [8–11].

The investigation of α-Al morphologies and their length-scales is regarded as critical for broadening the potential applications of cast Al-Ce alloys. Changing the Ce content and studying the morphologies in Al-Ce alloys, particularly when extremely high cooling rates (10^2 to 10^3 K/s) are obtained during rapid solidification processes, remain a key work to be realized.

Dendritic structures are more complex with more intricate branching and tend to generate different properties when compared to cellular ones. For instance, Canté et al. [12] showed that the Al-1.0 wt.% Ni alloy (dendritic) had a higher hardness than the Al-1.0 wt.% Fe alloy (cellular) because the morphology of the α-Al phase was more intricated. It was noted that dendritic growth made it possible to provide a more uniform distribution and alternation of the reinforcing phase.

Other studies did not mention the formation of cells in Al-Ce alloys, aside from the formation that was demonstrated by Martin et al. [13]. In this research, enhanced material properties were obtained by laser-based Al-Ce alloy fabrication, which was considered a route for an improved alloy. In this case, the development of very fine cells (1 to 2 μm in size) and nanometric intermetallics aided in the achievement. According to Brito et al. [14], in the literature for metallic systems, very few experimental studies on the growth of high velocity (or high cooling rate) cells can be found. The findings by Brito et al. [14] revealed the growth of high cooling rate cells followed by a dendritic region

formed under slower cooling conditions, signifying a reverse transition from dendrites to cells for an Al-Mg-Si alloy.

This paper aims to verify the effects of rapid solidification on the microstructures of the Al-4, 6 and 10.1 wt.% Ce alloys. The characteristics of the eutectic mixture and the growth of cells and dendrites have both been experimentally identified. The Ce content, eutectic fractions and α-Al morphologies have been examined in order to comprehend the tensile properties. Moreover, analytical modeling techniques were used to predict the solidification conditions that resulted in the Al-4 wt.% Ce alloy sample cells.

2. Materials and methods

Firstly, a master alloy was fabricated with a Ce content of approximately 16 wt.% Ce, according to chemical analysis by X-Ray Fluorescence (XRF) (EDX-720, Shimadzu). This alloy was melted in a crucible coated with zirconium oxide, using a Inductotherm PowerTrak induction furnace. Secondly, a sequence of melts dissolving such master alloy in Al generated the 3 alloys of interest, which went through an Argon degassing process for 2 minutes before being poured, to prevent gases trapped inside the alloy and the formation of defects. during solidification. Compositions were verified by X-Ray Fluorescence (XRF) resulting in Al-4, 6 and 10.1 wt.% Ce.

The same alloys were processed through a Titancast 700VAC centrifugal casting (Linn High Therm) in a hermetic chamber fixed perpendicularly to a rotation axis. The inductively molten alloys were driven into the Cu mold cavity by the force resulting from the rotation of the chamber (400 rpm). Samples at high solidification cooling rates with 4 mm thick plate geometry were produced.

Samples were polished and etched with a Keller's solution (HF 1%; HCl 1.5%; HNO_3 2.5% in water) for 5 s to reveal the cell/dendritic arrangements and etched with 15% HCl in water for 120 seconds to reveal the eutectic constituents. In order to obtain and analyze optical and scanning electron microscopy (SEM) images for samples of the 3 alloys, various specimens were cut throughout the cast plate transverse section. The intercept method was used to measure the microstructural spacing values along these portions [15]. For each tested alloy, at least 40 measurements were taken. SEM was also used to analyze the microstructure after the α-Al matrix was partially dissolved. Vickers microindentation hardness tests were carried out on the cross sections of the alloys using a test load of 500 g and a dwell period of 10 s. For each alloy, at least 20 hardness tests were performed. Both an optical microscope (BX14 M-LED, Olympus), and a Philips XL-30 FEG SEM were used.

At an initial strain rate of 3.0×10^{-3} s^{-1}, tensile strengths and elongations were examined for the tested alloys. An Instron 5969R machine with a 5000 N load cell and a calibrated video extensometer was used to conduct the tensile tests. Dogbone-shaped tensile specimens with gage lengths of 30 mm, widths of 4 mm, and thicknesses of 2 mm were machined for this purpose. The tensile tests were conducted in triplicate. It is worth noting that measurements of hardness, spacing and tensile tests were carried out with statistical rigor, with significant sampling for each condition.

3. Results and discussion

The presence of a branched α-Al phase dendritic network is observed for the Al-6 wt.% Ce and Al-10.1 wt.% Ce alloys, with this phase surrounded by the $Al_{11}Ce_3$/Al eutectic. The Al-4 wt.% Ce alloy, which exhibits predominantly cellular growth, is the exception in the observation of the three alloys, as can be seen in Fig. 1. The presence of primary phase $Al_{11}Ce_3$ particles in the microstructure of the Al-10.1 wt.% Ce alloy can be observed.

The formation of cells may be a result of the growth of thinner dendrites, which conform into cells, since nucleation and the growth of secondary arms are inhibited under these conditions [16]. This occurred preferentially for the lower solute content alloy (Al-4 wt.% Ce), by a reduction of instabilities in the side walls of the cells as compared to the other alloys with higher solute contents. Moreover, the addition of Ce generated a refining effect on the solidification structure, decreasing the secondary dendritic arm spacing, λ_2, with the increase in Ce from 4.0 to 10.1 wt.%. The λ_2 for these alloys changed from 4.7 to 3.2 μm. For the Al-4 wt.% Ce alloy the average cell spacing was 6.3 μm. Such refinement due to increase solute content was also observed for binary Al-Ni alloys under slow solidification (≈2 K/s). In this case, the λ_2 decrease from approximately 50 to 20 μm with increasing Ni content from 1.0 to 4.7 wt.% [9].

According to Dantzig and Rappaz [17], Al-Ce alloys are faceted/unfaceted systems with irregular Chinese Script eutectic morphologies, which differs from regular eutectics (lamellar or fibrous) in non-faceted/non-faceted systems due to the high melting entropy of the $Al_{11}Ce_3$ phase under equilibrium or close-to-equilibrium conditions. In contrast, particles with lamellar and fibrous morphologies were generated in the cell/interdendritic channels of the Al-Ce alloys produced by centrifugal casting, as can be seen in Fig. 2. This is due to the non-faceted growth of the $Al_{11}Ce_3$ phase possibly occurring during rapid solidification [18]. The coexistence of a mixture of fibers and lamellae was observed to occur for all tested alloys.

Hawksworth et al. [19] also observed a tendency of occurrence of breakdown from lamellar to a fibrous morphology at high solidification front velocities. They observed the same morphological transition aspect observed here for a solidification velocity of 5 mm/s, which is comparable in order of magnitude to that determined here.

Figure 3 shows the resulting tensile properties and hardness of the rapidly solidified samples as a function of Ce content. The length-scale of the eutectic, as small as 200 – 300 nm, along with their uniform distribution, and fine dendritic spacing all assist in enhancing the mechanical properties of the alloy. Both $Al_{11}Ce_3$ (≈350 HV) and α-Al (≈35 HV) generate an *in-situ* composite with the former acting as reinforcement.

Al-Ce alloys demonstrated improved yield and tensile strength but smaller elongation as the Ce content was increased. Refined $Al_{11}Ce_3$ particles offered high strengthening, and the Al-Ce alloys reached yield stresses higher than 86 MPa. Czerwinski et al. [20] demonstrated that the presence of coarse and mostly incoherent $Al_{11}Ce_3$ limited YS of just about 70 MPa. Typical cast production under

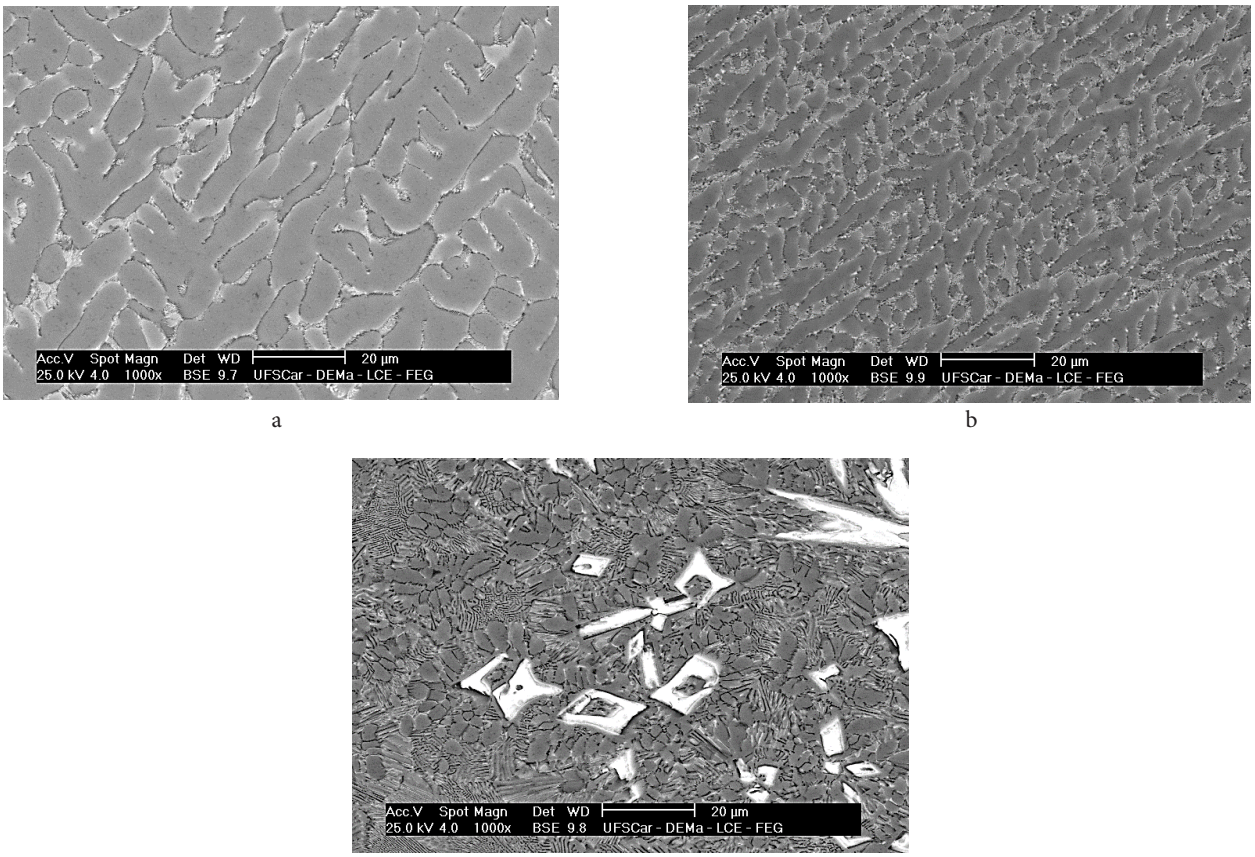

Fig. 1. Examples of SEM microstructures revealing the α-Al morphologies as a function of Ce content: Al-4 wt.% Ce (a), Al-6 wt.% Ce (b) and Al-10.1 wt.% Ce (c) alloys.

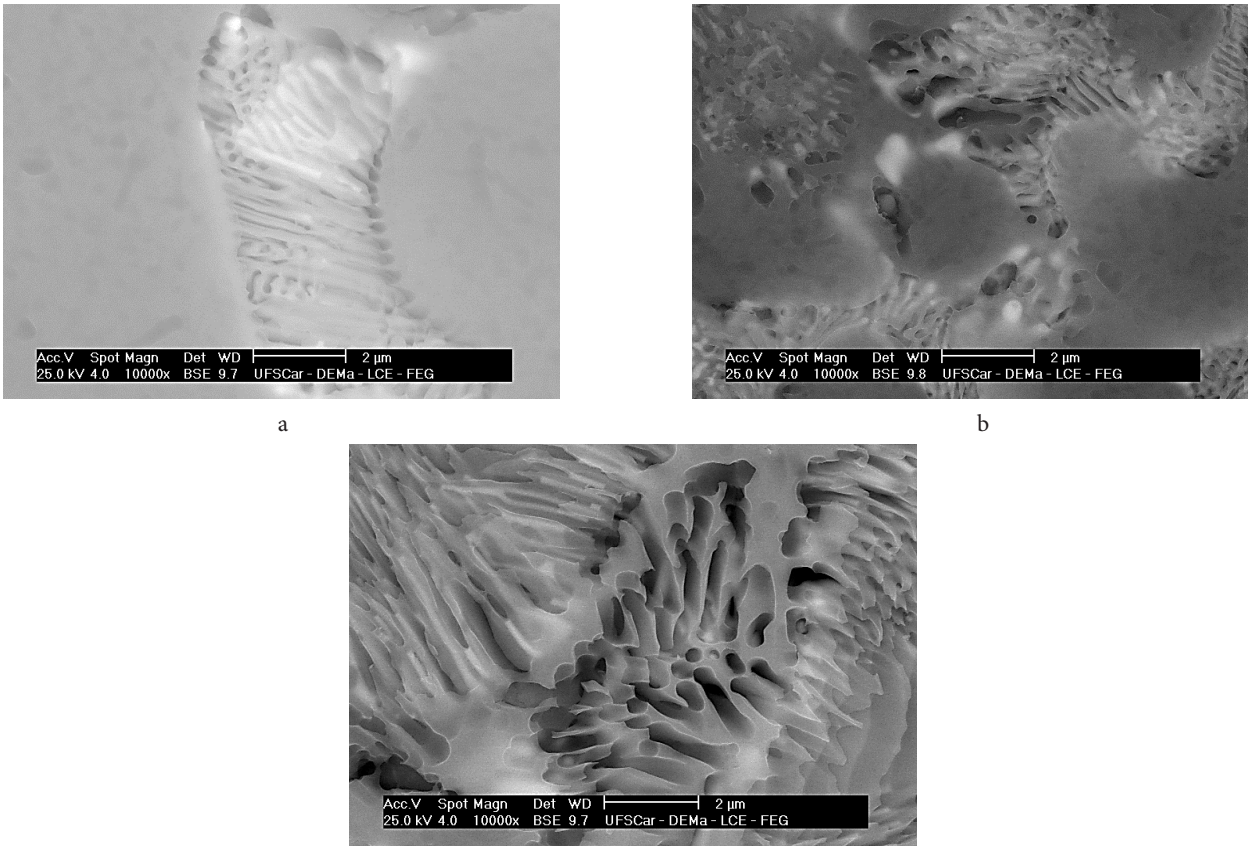

Fig. 2. Examples of intercellular and interdendritic constituents observed through SEM: Al-4 wt.% Ce (a), Al-6 wt.% Ce (b) and Al-10.1 wt.% Ce (c) alloys.

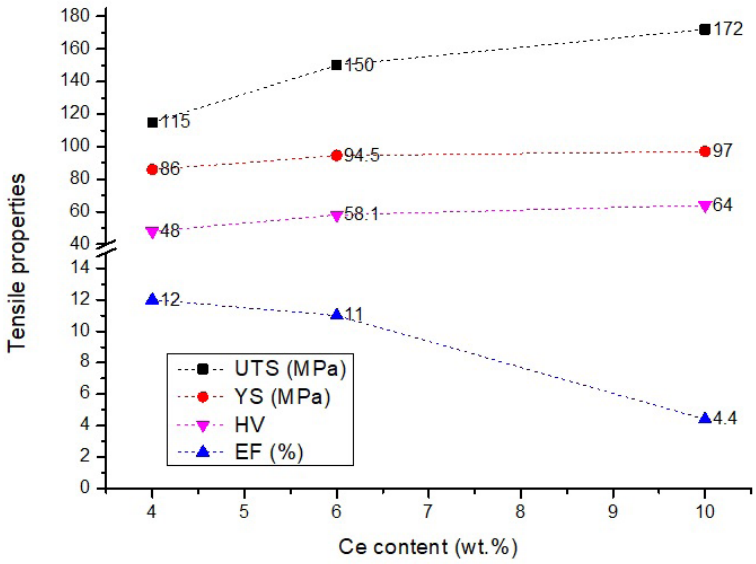

Fig. 3. (Color online) Average tensile properties and hardness as a function of Ce content for the Al-4, -6 and -10.1 wt.% Ce alloys. UTS — ultimate tensile strength, YS — yield strength, HV — hardness Vickers, EF — elongation-to-fracture.

slow solidification with the Al-6 and Al-10 wt.% Ce alloys poured into a 400°C pre-heated mold allowed YS values of 33 and 46 MPa [21], much lower than those attained here. Al-Ce alloys reported strengths are still insufficient for many commercial uses, hence new processing techniques are constantly needed. A promising alternative seems to be the centrifugal casting with Cu mold.

The predictive model proposed by Hunt and Lu for cell spacings assume solidification in unsteady-state heat flow conditions [22]. This model is able to calculate cell/dendritic spacings and undercooling. The theoretical model expression is shown in (1):

$$\lambda_c = 4.09 k_0^{-0.745} \left(\frac{\Gamma}{\Delta T}\right)^{0.41} D_L^{0.59} \nu_L^{-0.59}, \qquad (1)$$

where λ_c is the cell spacing, Γ is the Gibbs-Thomson coefficient, k_0 is the solute partition coefficient, D_L is the liquid solute diffusivity, ΔT is the difference between the liquidus and solidus equilibrium temperatures and ν_L is the cell tip growth rate. The upper limit should be twice the lower one, which is given by (1). Expressions like (1) showed good agreement with experiment at both low and high velocities [22], proving to be useful for comparing theory with experiment. Table 1 summarizes the employed thermophysical properties.

By predicting the solidification velocity during cell growth, ν_L, this model (1) was used to fit the experimental cell spacing. Following that, the cooling rate (CR) could be computed using the expression (2) [23]:

$$\mathrm{CR} = C_1 \times \nu_L^2, \qquad (2)$$

where C_1 is a constant value for a given alloy composition. Due to the similarities between Al-Ce and Al-Si microstructure maps demonstrated by Plotkowski et al. [7], a C_1 value of 1.6×10^7 K·s·m^{-2} for Al-Si [15] was adopted here.

Calculations of approximately 3.1 mm/s and 155 K/s were possible using the experimental λ_c of 6.3 μm. As-solidified centrifuged Al-based samples in Cu-molds have already been reported with values similar to those computed here [28]. The relationship between the cell-growth and the kinetic conditions observed here can thus be estimated through straightforward predictive modeling.

Table 1. Thermophysical properties of the Al-4 wt.% Ce alloy [25 – 28].

Property	Symbol [Units]	
Liquidus temperature	T_L [°C]	655.0
Eutectic Temperature	T_{Eut} [°C]	640.3
Partition coefficient	k_0	0.05
Gibbs-Thomson coefficient	Γ [mK]	3.5×10^{-8}
Solute diffusivity	D_L [m^{2}s^{-1}]	0.94×10^{-9}

4. Conclusions

In this study, optical microscopy, SEM, Vickers hardness, and tensile tests were used to characterize the centrifugal cast plates extensively. A strategy for evaluating cell growth conditions is suggested that is based on the combination of simple analytical modeling methods with experimental techniques.

The λ_2 spacing sensitive to the increased Ce content varying from 4.7 to 3.2 μm for Ce varying from 6.0 to 10.1 wt.% respectively. High cooling rate α-Al cells were shown to characterize the microstructure of a centrifuged-cast Al-4 wt.% Ce alloy in a Cu mold, having a eutectic mixture of $Al_{11}Ce_3$ fibers and lamellae filling the intercellular spacings. The experimentally determined cell spacing, $\lambda_c = 6.3$ μm, was inserted into the Hunt-Lu model with a view to permitting the solidification velocity (ν_L) to be determined: $\nu_L = 3.1$ mm/s. The solidification cooling rate (CR = 155 K/s) was then determined by an expression from the literature relating CR to ν_L.

Due to the effective microstructural refinement obtained by centrifugal casting, high YS values were obtained while

maintaining acceptable UTS and EF values. The presence of α-Al cells was identified in the Al-4 wt.% Ce alloy sample, resulting in relatively well-balanced tensile properties.

Acknowledgements: *The authors acknowledge FAPESP (grants 2019/23673-7 and 2022/06232-0) and CNPq. This study was financed in part by the Coordenação de Aperfeiçoamento de Pessoal de Nível Superior — Brasil (CAPES) — Finance Code 001.*

References

1. Y. Fan, M. Makhlouf. Metall. Mater. Trans. A. 46, 3808 (2015). Crossref
2. F. Czerwinski. Cerium in Aluminum Alloys. J. Mater. Sci. 55, 24 (2020). Crossref
3. F. Czerwinski. Mater. Sci. Technol. 36, 255 (2020). Crossref
4. L. Wang, R. Qi, B. Ye, Y. Bai, R. Huang, H. Jiang, W. Ding. Metall. Mater. Trans. A. 51,1972 (2020). Crossref
5. D. S. Ng, D. C. Dunand. Mater. Sci. Eng. A. 786, 139398 (2020). Crossref
6. L. Zhou, T. Huynh, S. Park et al. J. Mater. Sci. 55, 14611 (2020). Crossref
7. A. Plotkowski, O. Rios, N. Sridharan et al. Acta Mater. 126, 507 (2017). Crossref
8. P. R. Goulart, J. E. Spinelli, N. Cheung, A. Garcia. Mater Chem Phys. 119, 272 (2010).
9. M. V. Canté, J. E. Spinelli, N. Cheung, A. Garcia. Metals Mater Int. 16, 39 (2010).
10. W. R. Osório, L. C. Peixoto, M. V. Canté, A. Garcia. Mater Des. 31, 4485 (2010).
11. W. R. Osório, P. R. Goulart, A. Garcia. Mater Lett. 62, 365 (2008).
12. M. V. Canté, C. Brito, J. E. Spinelli, A. Garcia. Mater Des. 51, 342 (2013). Crossref
13. A. A. Martin, J. A. Hammons, H. B. Henderson, et al. Appl Mater Today. 22, 100972 (2021). Crossref
14. C. Brito, G. Reinhart, H. Nguyen-Thi et al. J Alloys Compd. 636, 145 (2015). Crossref
15. H. Kaya, E. Çardili, M. Gunduz. Appl Phys A. 94, 155 (2009).
16. W. Kurz, D. J. Fisher. Fundamentals of Solidification. Aedermannsdorf, Trans Tech Publications (1992) pp. 85 – 87.
17. J. A. Dantzig, M. Rappaz. Solidification. EPFL Press (2009).
18. B. Chanda, G. Potnis, P. P. Jana, J. Das. J. Alloy. Compd. 827, 154226 (2020). Crossref
19. A. Hawksworth, W. M. Rainforth, H. Jones. J Crystal Growth. 197, 286 (1999). Crossref
20. F. Czerwinski, B. Shalchi Amirkhiz. Materials. 20, 4549 (2020). Crossref
21. D. Weiss, O. Rios, Z. Sims, et al. Casting Characteristics of High Cerium Content Aluminum Alloys. In: Light Metals (ed. by A. Ratvik) The Minerals, Metals & Materials Series. Springer (2017). Crossref
22. J. D. Hunt, S. Z. Lu. Metall. Mater. Trans. A. 27A, 611 (1996). Crossref
23. J. E. Spinelli, A. A. Bogno, H. Henein. Metall Mater Trans A. 49, 550 (2018). Crossref
24. L. F. Mondolfo. Aluminum Alloys: Structure and Properties. Butterworths and Co., Ltd., London (1976) p. 806 Crossref
25. A. Juarez-Hernandez, H. Jones. J Crystal Growth. 208, 442 (2000). Crossref
26. H. Ohtani. The CALPHAD Method. In: Springer Handbook of Materials Measurement Methods (ed. by H. Czichos, T. Saito, L. Smith). Springer Handbooks, Springer, Berlin, Heidelberg (2006). Crossref
27. K. Sisco, A. Plotkowski, Y. Yang et al. Sci Rep. 11, 6953 (2021). Crossref
28. G. L. Gouveia, L. F. Gomes, N. Cheung et al. Adv Eng Mater. 23, 2001177 (2021). Crossref